Impact of misalignment on physics

G. Steinbrück[a]
for the ALICE, ATLAS, CMS and LHCb Collaborations

[a] *Institut für Experimentalphysik, Universität Hamburg*
Hamburg, Germany

Abstract
In this article we summarize the impact of misalignment of tracking detectors and muon systems on physics measurements. Studies from the ATLAS, CMS, and LHCb collaborations are presented.

12.1 Introduction

To exploit the enormous physics potential of the high luminosity environment at the LHC, highly segmented tracking detectors have been built by the LHC collaborations. In order to unambiguously identify particles in a dense environment and to measure their momenta and spatial coordinates precisely, these tracking devices have to be aligned well with respect to each other. The LHC collaborations have developed strategies to align their detectors. While tight constraints have been enforced during construction of the detectors, the final alignment precision can only be achieved using tracks from various beam and non-beam sources. To estimate the alignment needs, the experiments have studied in detail the effects misaligned detectors have on physics observables. These studies are summarized below.

12.2 Simulation of tracker misalignment

Both ATLAS and CMS have defined several scenarios which describe the amount of misalignment expected in various stages of the experiment [1,2]. Simulated data is produced with the detectors being misaligned according to these scenarios, and the impact on physics observables is studied. It should be noted that these scenarios are to be taken as benchmarks to test the alignment algorithms and the effects of residual misalignment on physics observables. They are guesses and should not be taken as a prediction of which level of alignment can be achieved exactly with a given luminosity.

Two levels of misalignment have been studied by CMS, The 'first data taking scenario' describes the amount of misalignment expected after a few months of data taking. The precision of the strip tracker alignment is determined by the mechanical precision during construction and the laser alignment system, yielding uncertainties in the 100 μm range, while the pixel detector is already assumed to be aligned to the 10 μm-range using tracks. The misalignment after first data taking is summarized in Tables 12.1 and 12.2, whereas the amount of misalignment for the CMS muon system is summarized in Table 12.3. The situation after more than six months of data taking is described in the 'long-term alignment' scenario. The alignment of the CMS strip tracker improves by a factor of 10, while the pixel tracker is assumed to already be aligned in the first step. Hence its alignment does not change between the two scenarios. The alignment of the muon system improves by a factor of 5 between the two scenarios.

Table 12.1: Expected misalignment after a few months of data taking (CMS)

	Δx $[\mu m]$	Δy $[\mu m]$	Δz $[\mu m]$	R_z $[\mu rad]$	LAS available
TPB	10	10	10	10	no
TIB	105	105	500	90	yes
TOB	67	67	500	59	yes
TPE	5	5	5	5	no
TID	400	400	400	100	no
TEC	57	57	500	46	yes

Table 12.2: Expected misalignment after a few months of data taking, substructures (CMS)

	TPB $[\mu m]$	TIB $[\mu m]$	TOB $[\mu m]$	TPE $[\mu m]$	TID $[\mu m]$	TEC $[\mu m]$
Modules	13	200	100	2.5	105	50
Ladders/Rods/Rings/Petals	5	200	100	5	300	100

Table 12.3: Expected misalignment for the CMS muon system after a few months of data taking

	Barrel		Endcap	
	Position [mm]	Orientation [mrad]	Position [mm]	Orientation [mrad]
Muon to tracker	1	0.2	1	0.2
Chambers	1	0.25	1	0.5

In their simulation ATLAS has introduced correlated misalignment in three levels: at the first level, the whole detector is misaligned to a few mm/a few tenths of a mrad. At the second level, large detector structures (layers and discs) are misaligned to 30–100 μm/0.5–1 mrad. At the third level, detector modules are misaligned to 30–150 μm/1 mrad. The results for CMS and ATLAS presented in the following sections refer to these misalignment scenarios.

12.3 Impact of misalignment on tracking and vertex finding

A misaligned tracking device can compromise physics observables through a deterioration in track quality and tracking efficiencies. Before looking at specific physics channels, the impact of misalignment on the performance of the tracking and vertex finding algorithms should be studied [3, 4].

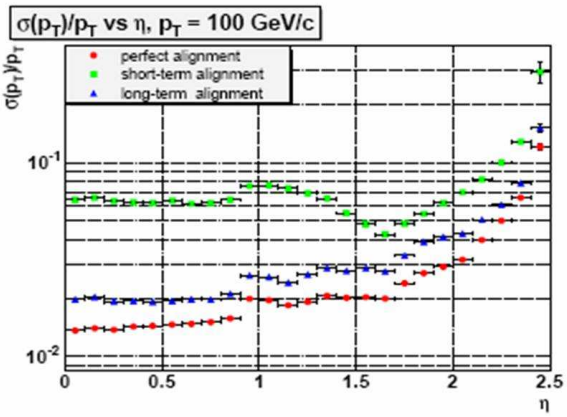

Fig. 12.1: Track p_t resolution as a function of pseudorapidity (CMS)

12.3.1 Tracking

Figure 12.1 shows the relative transverse momentum resolution for tracks in the CMS tracker as a function of pseudorapidity for the two levels of misalignment discussed above, and for a perfectly aligned tracker. A clear degradation in resolution can be seen. Likewise, Fig. 12.2 shows the impact of tracker alignment on the transverse impact parameter for the same CMS scenarios. Also, the tracking efficiency is shown in Fig. 12.3 as a function of pseudorapidity. If the errors are taken into account correctly, there is no visible impact of the levels of misalignment studied here on the tracking efficiency. Of course, if the hit resolutions get enlarged such that additional ambiguities are introduced as to which hits are associated with a track, the tracking efficiencies will also suffer.

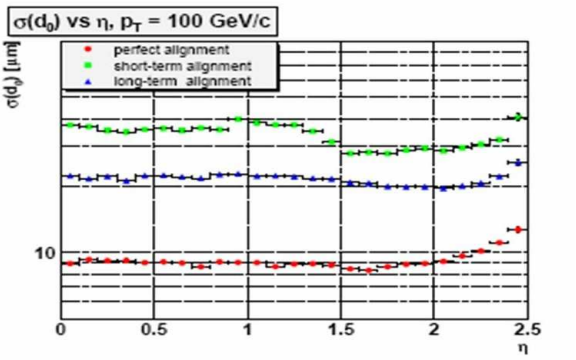

Fig. 12.2: Transverse impact parameter resolution as a function of pseudorapidity (CMS)

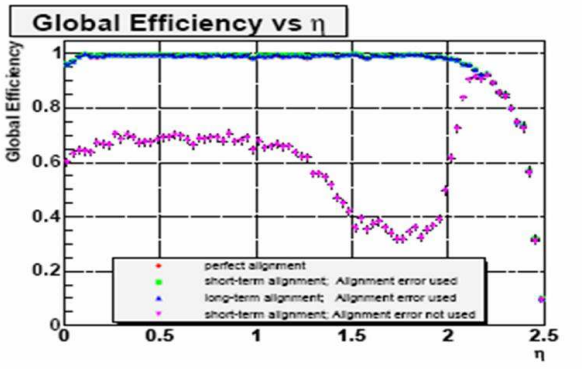

Fig. 12.3: Track efficiencies for various levels of misalignment (CMS). Also shown is the tracking efficiency for the short-term misalignment scenario if increased hit position errors are not taken into consideration.

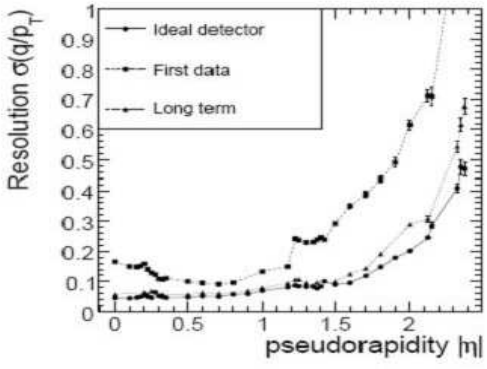

Fig. 12.4: Muon $1/p_t$ resolution as a function of pseudorapidity (CMS)

Table 12.4: Expected impact of misalignment on vertex finding (CMS)

X- and Y-coordinates					
	$\sigma_{x,y}$ [μm]	95% coverage [μm]	Bias [μm] X	Bias [μm] Y	$Pull_{x,y}$
Perfect tracker alignment					
$B_s^0 \to J/\psi\phi$	45	119	-0.5 ± 0.6	-0.6 ± 0.6	1.15
$t\bar{t}H$	10	26	-0.0 ± 0.2	0.1 ± 0.2	1.16
DY	13.5	46	0.2 ± 0.3	-0.5 ± 0.3	1.12
Short-term tracker alignment					
$B_s^0 \to J/\psi\phi$	51	128	-5.8 ± 0.7	12 ± 0.7	1.16
$t\bar{t}H$	18	47	2.4 ± 0.2	16 ± 0.2	1.48
DY	24	62	1.6 ± 0.4	16 ± 0.4	1.23
Long-term tracker alignment					
$B_s^0 \to J/\psi\phi$	51	127	-10 ± 0.7	11 ± 0.7	1.16
$t\bar{t}H$	17	47	-9.5 ± 0.4	11 ± 0.4	1.46
DY	22	59	-8.9 ± 0.4	11 ± 0.4	1.28

CMS has also studied the impact of combined misalignment of the tracking detectors and the muon system on high transverse momentum muons (1 TeV), a range where both the tracker and the muon system contribute to the momentum measurement.

Figure 12.4 shows the relative resolution in $1/p_{\mathrm{t}}$ as a function of pseudorapidity for the three levels of combined misalignment. A clear degradation of the p_{t} resolution can be observed if the tracking detectors and the muon system are misaligned.

12.4 Vertex finding and fitting

CMS has studied the impact of a misaligned tracker on vertex finding and fitting. Table 12.4 compares vertex resolutions and biases for the vertex finding step for three benchmark physics processes, $B_S \to J/\psi\phi$, $t\bar{t}H$, and Drell–Yan production, covering different momentum ranges and both primary and secondary vertices. Again, the three reference scenarios described earlier are used as benchmarks. While the impact on vertex finding efficiencies (not shown here) is small, a clear degradation in the vertex resolution in x and y can be seen when comparing a perfectly aligned tracker to the short-term scenario. The difference between the short-term scenario and the long-term scenario is small for low p_{t} tracks as present in the B_s sample. This is due to the fact that the misalignment of the pixel tracker is assumed to be the same for both scenarios, while the strip tracker alignment improves by a factor of 10. For higher momentum tracks as present in the Drell–Yan and the Higgs samples, the strip tracker contributes to the vertex measurement and some improvement can be seen. Apart from the degradation of vertex resolutions caused by random misalignment, systematic misalignments of larger substructures can cause biases in the vertex position that can be harmful in many physics measurements.

After the vertex finding step, vertex positions are refit using a Kalman filter algorithm. Table 12.5 again compares benchmark observables for fitted vertices for the same scenarios and physics channels. Here, the results are shown separately for the primary and the secondary vertices for the B_s sample. For secondary vertices, a difference of 12 μm can be seen in all coordinates.

12.5 The impact of misalignment on physics measurements

In the following sections, specific benchmark physics channels are analysed with respect to their sensitivity to misalignment.

Table 12.5: Expected impact of misalignment on vertex fitting (CMS)

	x-coordinate				z-coordinate			
	Res. Std. Dev. [μm]	Res. Mean [μm]	95% Cov. [μm]	Pull	Res. Std. Dev. [μm]	Res. Mean [μm]	95% Cov. [μm]	Pull
Perfect tracker alignment								
$B_s^0 \to J/\psi\,\phi$ SV	54.2	0.545	164	1.09	72.6	-0.718	445	1.08
$B_s^0 \to J/\psi\,\phi$ PV	43.8	0.596	176	1.11	54	0.633	223	1.07
$t\bar{t}H$	13.5	-0.299	106	1.45	17.2	-0.0625	116	1.43
Short-term tracker alignment								
$B_s^0 \to J/\psi\,\phi$ SV	66.6	-2.5	190	1.12	84	1.82	519	1.08
$B_s^0 \to J/\psi\,\phi$ PV	49.5	-8.16	233	1.16	57.7	-2.32	282	1.07
$t\bar{t}H$	24.3	0.69	205	1.97	24.3	1.79	244	1.58
Long-term tracker alignment								
$B_s^0 \to J/\psi\,\phi$ SV	63.8	-10.9	177	1.09	80.5	-3.86	502	1.07
$B_s^0 \to J/\psi\,\phi$ PV	47.9	-10.8	187	1.13	57.2	-4.86	233	1.06
$t\bar{t}H$	20.9	-11.6	116	1.83	22.3	-4.25	129	1.56

12.5.1 Dimuon resonances: Higgs searches

Lepton pairs lead to clean experimental signatures in Standard Model physics and in searches beyond the Standard Model. An example is the possibility to detect the Higgs boson in the channel $H \rightarrow ZZ \rightarrow llll$, which becomes important if the mass of the Higgs boson is above the threshold for producing Z boson pairs. Figure 12.5 shows the p_{t} resolution of muons in $H \rightarrow ZZ \rightarrow \mu\mu ee$ events for the three CMS benchmark scenarios, while the dimuon mass resolution is shown in Fig. 12.6. Excellent alignment is needed if the effect of misalignment should be negligible. Figure 12.7 shows the reconstruction efficiency as a function of dimuon invariant mass, while the dimuon mass resolution is shown in Fig. 12.8. Again, the impact on the offline reconstruction efficiency is small, while the mass resolution suffers strongly, especially at high mass: in comparison to a perfectly aligned tracker, the mass resolution at 1 TeV is enlarged by a factor of 1.3 and 3 for the long-term and first data scenario, respectively. At 3 TeV, the corresponding factors are 1.4 and 5, respectively.

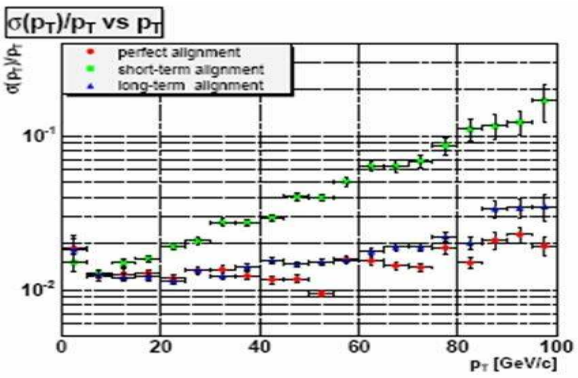

Fig. 12.5: Relative p_{t} resolution as a function of p_{t} for muons in $H \rightarrow ZZ \rightarrow \mu\mu ee$ decays. Compared are the three aforementioned misalignment scenarios (CMS).

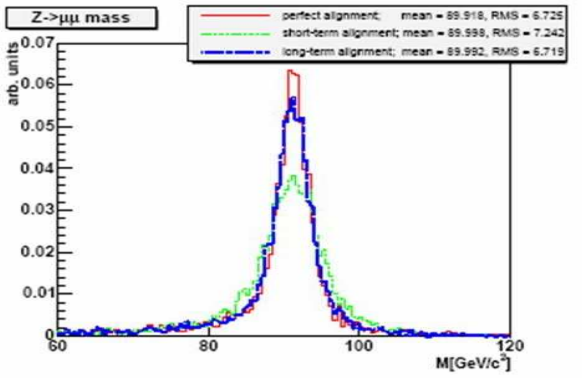

Fig. 12.6: $Z \rightarrow \mu\mu$ mass peak (right) for the same sample (CMS). Compared are the three aforementioned misalignment scenarios.

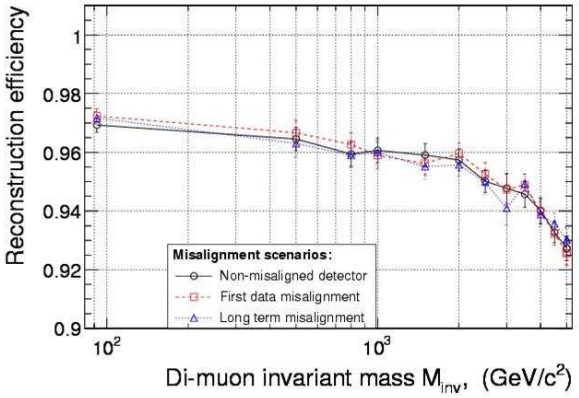

Fig. 12.7: Reconstruction efficiency as a function of dimuon mass (CMS)

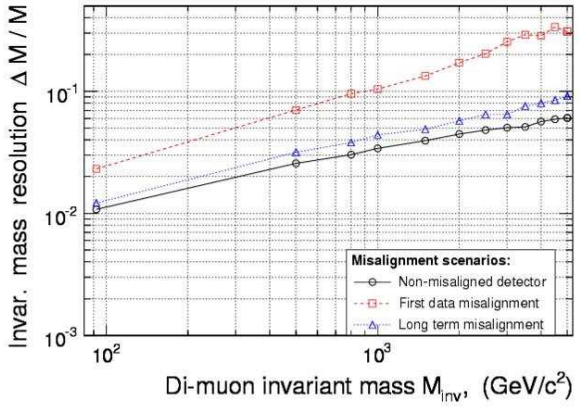

Fig. 12.8: Dimuon invariant mass resolution as a function of dimuon mass (CMS)

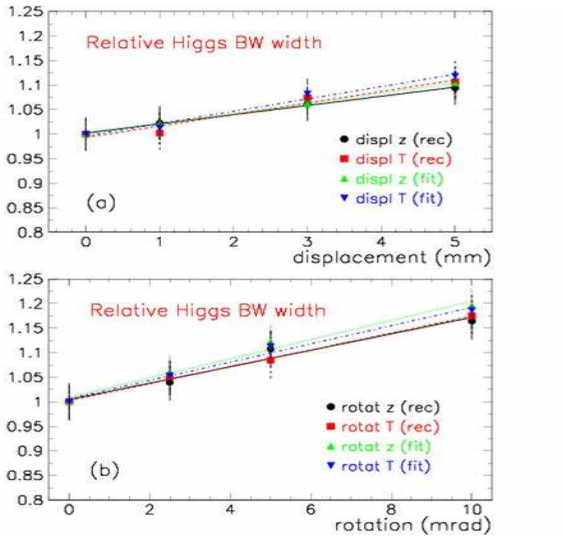

Fig. 12.9: Higgs width (Breit–Wigner) for displacements (above) and rotations (below) (ATLAS)

12.5.2 $H \rightarrow 4\mu$: The impact of muon system misalignment

ATLAS has studied the effect of a relative misalignment of the end-cap to the barrel muon system in the channel $H \rightarrow ZZ \rightarrow \mu\mu\mu\mu$ [5]. Figure 12.9 shows the widths of the Higgs resonance obtained by fitting a Breit–Wigner function to the four-muon spectrum, as a function of displacements and rotations. Likewise, in Fig. 12.10 the dependence of the acceptance for these events is shown as a function of displacement and rotation. A linear dependence of the width and the acceptance on the muon system misalignment can be observed. As an example, the resolution is increased by 10% at an angle of 5 mrad, while the acceptance is specially sensitive to rotations around the x-axis.

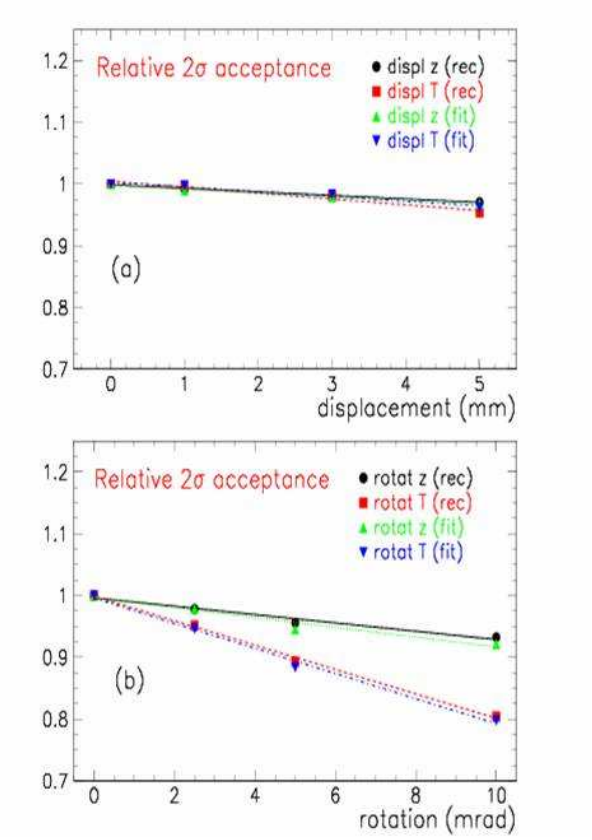

Fig. 12.10: Acceptance for $H \rightarrow 4\mu$ events as a function of displacements (above) and rotations (below) (ATLAS)

12.5.3 Searches for physics beyond the Standard Model in dimuon events

Dimuons can directly be produced in the decay of extra heavy Z bosons (Z′) and in the decay of Randall–Sundrum gravitons, which appear in models of extra spatial dimensions. Figure 12.11 shows the integrated luminosity needed for a 5 σ discovery of a Z′ as a function of the mass of the Z′. Different Z′ models are compared. For the mass point of 1 TeV, the short-term alignment is used, since very little integrated luminosity is needed to reach 1 TeV ($\approx$ 15–100 pb^{-1}). Similarly, the integrated luminosity needed for a 5 σ discovery of a Randall–Sundrum graviton is shown in Fig. 12.12. The effect of short-term misalignment is shown for comparison. If optimal alignment is achieved, about 50% less data is needed for the same level of significance. The dimuon mass resolution for a 1 TeV Randall–Sundrum graviton is shown in Fig. 12.13 for several levels of tracker and muon system misalignment. Likewise, Figure 12.14 shows the same for a 3 TeV graviton, but this time only long-term alignment is shown due to the fact that at the luminosity needed for discovery of such a massive particle, the level of understanding of the alignment will be fairly advanced.

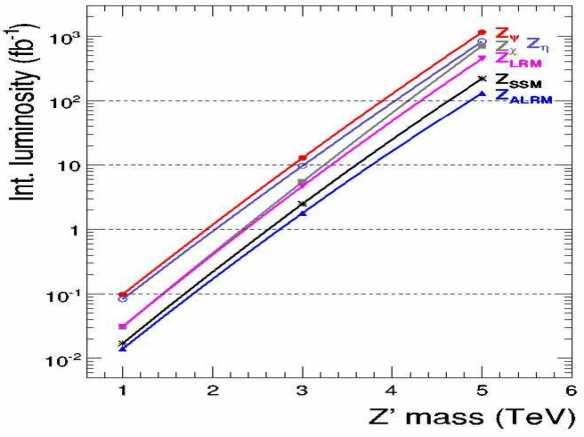

Fig. 12.11: Integrated luminosity needed for 5 sigma discovery for different Z′ models (CMS)

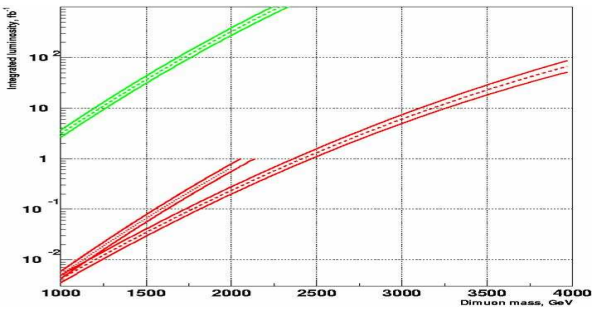

Fig. 12.12: Integrated luminosity for 5 sigma discovery for a Randall–Sundrum graviton (CMS). The upper curve is for a coupling constant of C = 0.01, while the lower curves assume C = 0.1. The upper branch of the lower curve is for short-term alignment, while the main curve assumes long-term alignment.

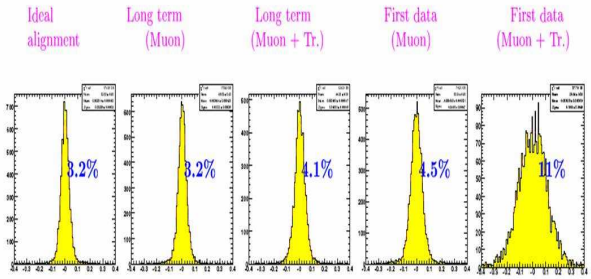

Fig. 12.13: Dimuon mass resolution for 1 TeV Randall–Sundrum gravitons, various levels of misalignment (CMS)

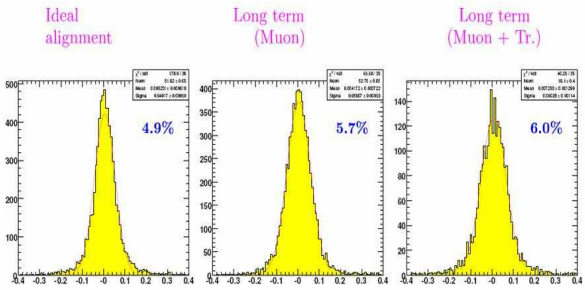

Fig. 12.14: Dimuon mass resolution for 3 TeV Randall–Sundrum gravitons, various levels of misalignment (CMS)

12.5.4 The measurement of the W boson mass

The measurement of the W boson mass is one of the most challenging precision measurements at the LHC due to the high level of detector understanding needed to go beyond the precision reached at the Fermilab Tevatron. The muon channel, where the momentum measurement is dominated by the tracking detectors, is especially sensitive to effects of misalignment, while in the electron channel the energy/momentum scale comes both from the tracker and the calorimeter. CMS and ATLAS have studied the impact of misalignment of the tracking on the W mass measurement and the level of alignment needed for the W boson mass measurement. CMS finds that for an initial measurement with 1 fb^{-1} of data, the contribution to the W mass uncertainty due to misalignment is in the order of 10 MeV (see Table 12.6). In the long run, the effect of misalignment is thought to be negligible, with a good level of tracker alignment being assumed. ATLAS estimates that the momentum scale ($1/p_{\mathrm{t}}$) of the inner detector has to be understood to the 0.02% level for the W mass measurement [1]. This precision can only be obtained in a relative calibration against the Z boson mass. While most of the momentum scale uncertainty vanishes using this method, residual uncertainties remain, which are difficult to quantify exactly. ATLAS estimates that these translate into alignment requirements in the order of 1 μm in rϕ, 10 μm in R, and 10 μm in z in the pixel detector. The tracker has to be stable to that level for more than a day. These tight requirements are to be compared to the ATLAS general requirements of 7 μm for the pixel tracker and 12 μm for the silicon strip tracker. On the other hand, ATLAS is optimistic that they can control the alignment to the level required here. Table 12.7 lists the alignment uncertainties obtained after one day of low luminosity running in the rϕ coordinate for different sources of tracks.

Table 12.6: W mass uncertainties, CMS. The left two columns list the level of understanding and the contribution to the W mass uncertainty in MeV for 1 fb^{-1} of data. The right two columns are for 10 fb^{-1} of data.

transformation method applied to W$\rightarrow \mu\nu$				
statistics		40		15
background	10%	4	2%	negligible
momentum scale	0.1%	14	<0.1%	<10
$1/p^T$ resolution	10%	30	<3%	<10
acceptance definition	η-resol.	19	$< \sigma_\eta$	<10
calorimeter $E_{\mathrm{T}}^{\mathrm{miss}}$, scale	2%	38	$\leq$1%	<20
calorimeter $E_{\mathrm{T}}^{\mathrm{miss}}$, resolution	5%	30	<3%	<18
detector alignment		12	–	negligible
total instrumental		64		<30
PDF uncertainties		$\approx$20		<10
Γ_W		10		< 10

Table 12.7: Alignment precision after one day of low luminosity running (ATLAS)

Table 2-2 Rϕ alignment precisions (μm) which can be obtained after one day of low luminosity running. Results are given for different types of tracks, using both complete modules and the Rϕ overlaps.

Type of Track	Pixels				SCT			
	Barrel		End-cap		Barrel		End-cap	
	Module	Overlap	Module	Overlap	Module	Overlap	Module	Overlap
$W \rightarrow \mu\nu$	1.0		1.2		2		1.3	
Single muons	0.4	2.4	0.4	4	0.7	7	0.5	5
Low-p_T tracks		0.7		0.9		1.5		1.0

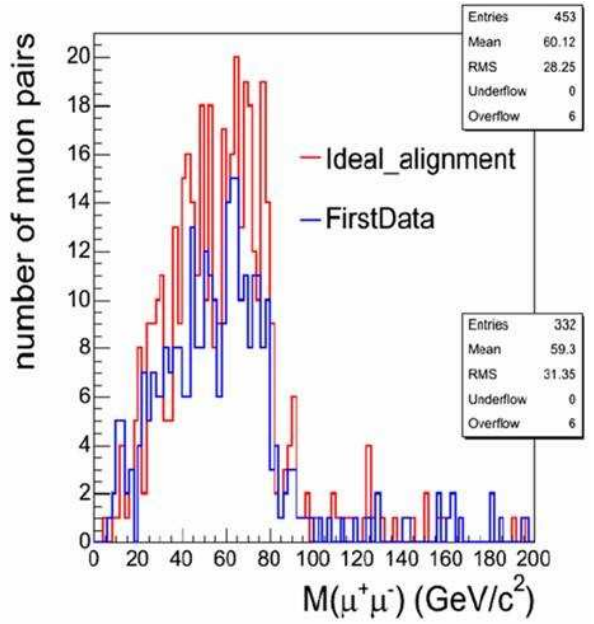

Fig. 12.15: Dimuon invariant mass for $\chi_2^0 \rightarrow \chi_1^0\mu\mu$ with and without misalignment (CMS)

12.5.5 Supersymmetry

Supersymmetry is one of the most promising extensions of the Standard Model of high-energy physics and the prospects for discovering supersymmetry at the LHC are excellent over a large mass range, provided it is realized in Nature. After a discovery of signatures consistent with supersymmetry, the mass spectra of supersymmetric particles have to be studied to distinguish different models. As an example, the decay of higher into lower mass neutralinos and pairs of leptons is discussed here. In some regions of mSUGRA parameter space (higher mass) neutralinos are produced from the decay of squarks and gluinos. These can decay into lighter neutralinos and same-flavour-opposite-sign lepton pairs, according to $\chi_2^0 \rightarrow \chi_1^0 ll$. The dilepton invariant mass spectrum exhibits a characteristic endpoint given by the mass difference of the two neutralinos.

CMS has analyzed the ability to observe this endpoint in reconstructed events, comparing results for a misaligned tracker to perfect alignment. For a tracker misaligned to a level assumed in the first data scenario, the end point is still visible, with a shift of about 1 GeV. However, the event selection efficiencies are reduced significantly: for the dielectron channel they decrease by 10% and 2% for the first data and long-term scenarios, respectively. For the dimuon channel the effect is even larger with 13% and 30%, respectively, if the muon system is misaligned as well. Figure 12.15 shows the dimuon mass spectrum with and without misalignment.

12.5.6 B physics

B physics relies on precise tracking in reconstructing B mesons. LHCb has studied misalignment of the VELO detector (vertex locator) in detail [6, 7]. The alignment of the VELO is potentially an issue due to its special buildup: the two halves of the VELO are retractable from the beam pipe during fills (see Fig. 12.16). LHCb has studied both uncorrelated misalignment of modules and correlated misalignment of a whole box (VELO half).

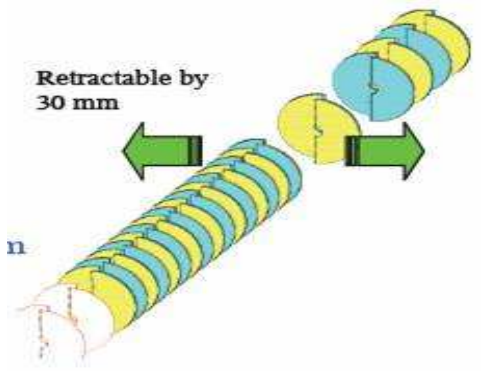

Fig. 12.16: The LHCb VELO detector

The impact parameter resolution for different levels of box misalignment is shown in Fig. 12.17. It deteriorates with increasing misalignment, specially for large track momentum. The impact parameter is directly

related to the proper time, hence the proper time measurement would be degraded. Since misalignment leads to a worse momentum resolution, misalignment directly affects the mass resolution in $B_S \rightarrow \pi^+K^-$ decays. Figure 12.18 shows the widening of the mass spectrum for momentum resolutions of 0.4%, 0.5%, and 0.7%, respectively. The width of the B_S peak increases from 13 MeV to 20 MeV and 26 MeV, respectively. Note that with increasing widths of the B_S signal peak, the B_d peak (background) increases as well, and the background/signal grows (see Fig. 12.19).

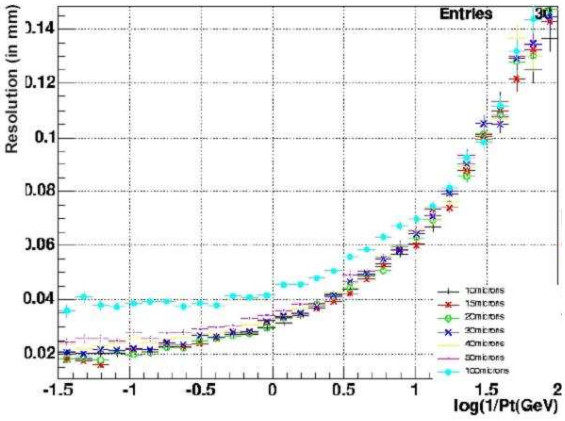

Fig. 12.17: Impact parameter resolution for LHCb VELO box misalignment in x (10–100 μm).

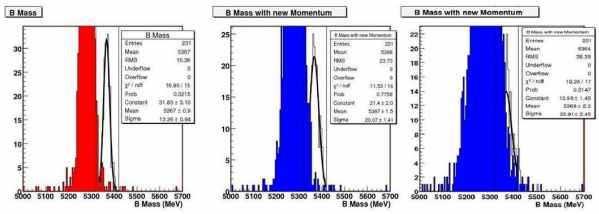

Fig. 12.18: $B_S \rightarrow \pi^+K^-$ mass resolution as a function of momentum resolution

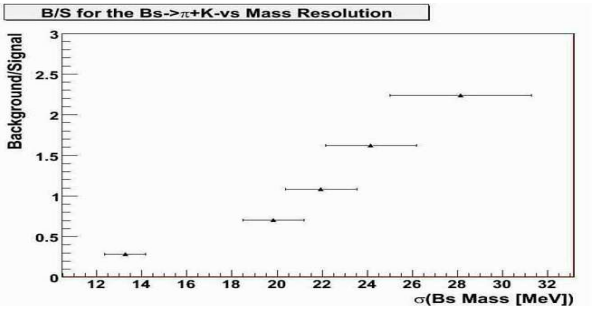

Fig. 12.19: Background/signal for $B_S \rightarrow KK$. The background considered is $B_d \rightarrow K^+\pi^-$.

The ability to distinguish signal from background is especially important in the search for rare B decays. One example is the decay $B_S \rightarrow \mu\mu$, which is forbidden in the Standard Model at tree level as it would only be possible through flavour changing neutral currents. In the Standard Model, this process is only possible through penguin and box diagrams, which are strongly helicity suppressed (see Fig. 12.20). The expected branching ratio is 3.4×10^{-9} while branching ratios above 4.1×10^{-7} are experimentally excluded at the moment. Figure 12.21 shows the $S/\sqrt{S+B}$ as a function of the mass window used in the LHCb analysis for different momentum resolutions. As discussed above, the momentum resolution directly affects the ability to distinguish signal from background, which will in turn determine the experimental limit that can be set on such a rare process.

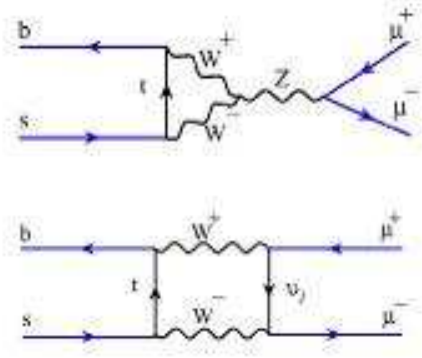

Fig. 12.20: Feynman diagrams for $B_S \rightarrow \mu\mu$

In contrast to ATLAS and CMS, LHCb relies on its silicon tracking detector in the Level 1 trigger. Figure 12.22 shows the trigger efficiency for $B_S \rightarrow KK$ events and the rejection for minimum bias tracks as a function of rotation around the y-axis. The level 1 trigger efficiency is reduced by 50% for a rotation of 0.7 mrad around the y axis.

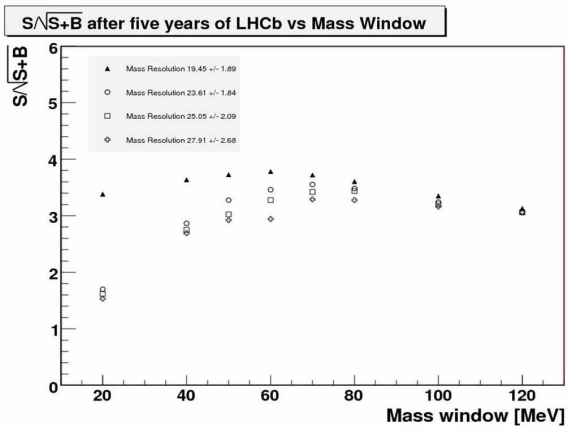

Fig. 12.21: $Signal/\sqrt{Signal + Background}$ for $B_S \rightarrow \mu\mu$

As a benchmark B-physics channel, CMS has also studied the effect of misalignment on $B_S \rightarrow \mu\mu$ events (see Fig. 12.23). The B_S mass resolution increases from 45 MeV for a perfectly aligned detector to 49 and 54 MeV for the long-term and short-term scenario, respectively (see Fig. 12.23).

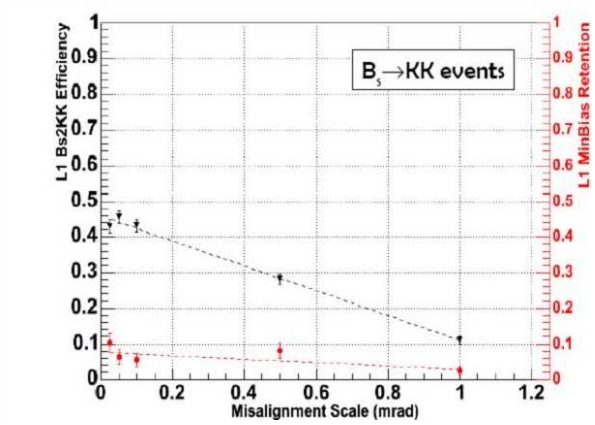

Fig. 12.22: Trigger efficiency for $B_S \rightarrow KK$ events as a function of VELO rotation

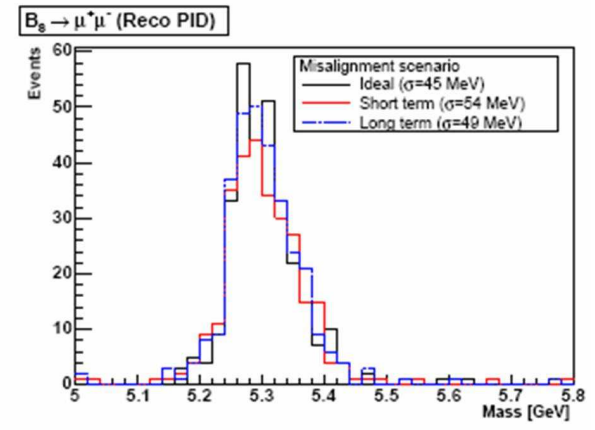

Fig. 12.23: Dimuon invariant mass for $B_S \rightarrow \mu\mu$ events for three levels of misalignment (CMS)

12.5.7 B tagging

The performance of a b-tagging algorithm is directly affected by misalignment due to the loss in separation of displaced tracks from tracks originating from the primary vertex. ATLAS has studied the rejection power of their 3-D b-tagging algorithm for three levels of misalignment. Compared are the absolute rejection power with respect to light jets for two reference b-tagging efficiencies (50% and 60%), and the relative rejection power normalized to the values for no misalignment. The results summarized in Table 12.8 show a strong dependence of the b-tagging performance on misalignment.

Table 12.8: Degradation of b tagging performance with misalignment (ATLAS)

		$R_0 = R_u$ perfect alignm.	R_u $\sigma_{R\phi} = 5\mu$m $\sigma_z = 15\mu$m	R_u $\sigma_{R\phi} = 10\mu$m $\sigma_z = 30\mu$m	R_u $\sigma_{R\phi} = 20\mu$m $\sigma_z = 60\mu$m
3D	ϵ_b=50%	262 ± 8	259 ± 8	237 ± 7	175 ± 4
	ϵ_b=60%	81 ± 1	79 ± 1	74 ± 1	57 ± 1
		R_u/R_0	R_u/R_0	R_u/R_0	R_u/R_0
3D	ϵ_b=50%	1.00	0.99	0.91	0.67
	ϵ_b=60%	1.00	0.97	0.92	0.71

12.6 Summary

In summary, the ATLAS, CMS, and LHCb collaborations have studied in detail the impact of misaligned tracking detectors and their muon system on measurements of physics quantities. Many measurements are compromised by misaligned detectors. To exploit the physics potential of the LHC, excellent alignment is required. While a challenge to the alignment algorithms, studies have shown that the desired levels of alignment can be reached.

Acknowledgements

We wish to thank Ashfaq Ahmad, Steve Blusk, Oliver Buchmüller, Tobias Golling, Sergio Gonzales, Daniel Levin, Francisco Matorras, Jacopo Nardulli, Jochen Schieck, Maria Spiropulu, Peter Schleper, Markus Stoye, and Sebastien Viret who provided material and valuable input for this talk.

References

[1] ATLAS Collaboration, CERN/LHCC 1999-014 (1999).

[2] I. Belotelov *et al.*, CMS Note 2005/036 (2005).

[3] CMS Collaboration, CERN/LHCC 2006-001 (2006).

[4] P. Vanlaer *et al.*, CMS Note 2006/029 (2006).

[5] G. Avolia, ATL-MUON-2001-001 (2001).

[6] D. Petrie, C. Parkes, and S. Viret, LHCb-2005-056 (2005).

[7] `http://ppewww.physics.gla.ac.uk/LHCb/VeloAlign/` .